Journal of Colloid and Interface Science **251,** 131–142 (2002)
doi:10.1006/jcis.2002.8363

Application of the Charge Regulation Model to Transport of Ions through Hydrophilic Membranes: One-Dimensional Transport Model for Narrow Pores (Nanofiltration)

W. B. Samuel de Lint,*,[1] P. Maarten Biesheuvel,† and Henk Verweij‡

*Inorganic Materials Science Group, Department of Chemical Technology, & Mesa+ Research Institute, University of Twente, P.O. Box 217, 7500 AE Enschede, The Netherlands; †Laboratory of Physical Chemistry and Colloid Science, Wageningen University, Dreijenplein 6, 6703 HB Wageningen, The Netherlands; and ‡Department of Materials Science and Engineering, The Ohio State University, 2041 College Road, 291 Watts Hall, Columbus, Ohio 43210-1178

Received October 29, 2001; accepted March 15, 2002; published online June 3, 2002

The charge regulation concept is combined with the Navier-Stokes and Nernst-Planck equations to describe the ion retention of nanofiltration membranes consisting of narrow cylindrical pores. The charge regulation approach replaces the assumption of a constant charge or a constant potential at the membrane pore surface, and accounts for the influence of pH, salt concentration, and type of electrolyte on ion retention. In the current model, radial concentration and potential gradients are considered to be negligibly small (valid for narrow enough pores), resulting in a one-dimensional transport description. The model describes typical experimental data for nanofiltration membranes, such as the change of ion retention with pore radius, ion concentration, pH, and pressure both for monovalent and multivalent ions. For a constant solvent velocity, the model in some cases predicts an optimum pore size for retention. Nonequal retentions for anions and cations are predicted at low and high pH values, as well as a minimum solvent velocity for very low salt concentrations. For higher salt concentrations, and at a fixed pressure difference, an increase in solvent velocity with increasing ion concentrations is predicted, in agreement with other one-dimensional transport descriptions found in the literature, but in contrast to some experimental data.

Key Words: **charge regulation; Nernst-Planck; mass transport; membranes; nanofiltration; ion exchange.**

INTRODUCTION

Nanofiltration (NF) membranes consist of a thin separation layer with pore sizes in the 1–10 nm range, in between the pore sizes of reverse osmosis and ultrafiltration membranes. NF membranes can separate ions from aqueous solutions using electrostatic effects and typically have higher solvent fluxes, but lower retentions, than reverse osmosis membranes.

Theoretical studies on mass transport in NF membranes use different approaches, such as derivative models from the Generalized Maxwell-Stefan (GMS) theory (1–11), the concept of hydrodynamics (12), a combination of both (13, 14), or irreversible thermodynamics (15, 16). We use the GMS description, which simplifies to the Nernst-Planck (NP) equation for dilute systems (17). Combining the NP approach with proper descriptions of momentum transfer (Navier-Stokes), electrostatics (Poisson), continuity of mass, electroneutrality, zero electric current, and the interactions with the membrane material suffices to completely specify the mass transport of ions. Because solving the full NP and Poisson equations for the complex structure of a membrane is mathematically formidable, simplifications of the governing relations are very useful. Therefore we assume the membrane to be constructed of a collection of straight capillary pores with a small and uniform radius. For small enough pore radii radial gradients in the electrostatic potential and the concentration of ions can be neglected (9, 10, 13, 14).

To understand the ion retention behavior of NF membranes as a function of feed solution conditions, pressure, and surface charge, mass transport of the ions and solvent through the membrane pore as well as chemical interactions with the membrane pore surface must be considered. Transport descriptions for NF membranes generally assume a constant surface potential or surface charge (1, 2, 5–9, 13, 14). However, it is known from practice as well as from theory that the surface charge and surface potential change with pH, salt concentration, and the extent of electrostatic double-layer overlap (like in narrow pores) because of the specific interaction of ions in solution with the pore surface (18–23); these effects are considered in the charge regulation (CR) approach (24–27). For charged membranes, Jacazio *et al.* (2) and Westermann-Clark *et al.* (8) were the first to realize this dependence of surface charge on material and solution properties, though they did not incorporate the ion-surface interactions in their model description. Bowen *et al.* (12) used a Freundlich-like isotherm to determine a homogeneous membrane charge density as a function of the ion concentrations in the feed and found no influence of the type of electrolyte. Sasidhar *et al.* (28) and Takagi *et al.* (29) followed the same approach and used a Langmuir isotherm to describe specific adsorption of counterions at the membrane surface.

[1] To whom correspondence should be addressed. Fax: +31 53 489 4683. E-mail: w.b.s.delint@ct.utwente.nl.

0021-9797/02 $35.00

Similar to (12), Takagi *et al.* (29) related the Langmuir adsorption parameters to the feed concentrations of the species. Basu *et al.* (3) integrated the charge regulation concept into a space-charge model for transport through microporous mica, but they did not focus on the separation properties of the material. Like Basu *et al.* (3), Hall *et al.* (18, 19) combined charge regulation with mass transport, but focused more on retention behavior, see also (20). Also, the transport of hydroxyl ions and protons was explicitly accounted for in (18–20). In the work of Hall *et al.* (18, 19) the charge regulation adsorption parameters were obtained by fitting the model to membrane retention data of binary electrolyte solutions. Starov *et al.* (20) used charge regulation data (18, 19) in a homogeneous mass transport model. In a previous effort (21), we used the charge regulation concept for a pore at thermodynamic equilibrium to describe the increase of retention with decreasing pore size and the decrease of retention when the pH approaches on the isoelectric point (IEP). In the present effort the equilibrium model (21) is extended by combining the charge regulation approach with the Nernst-Planck equation, the Navier-Stokes equation, and continuity of mass to predict the ion separation behavior of a hydrophilic NF membrane. The membrane is modeled as a collection of cylindrical pores with the pore-mouths on both sides of the membrane at thermodynamic equilibrium with the adjacent solution phase. Furthermore, we assume the pore radius small enough for the radial concentration and potential gradients to be negligibly small (uniform potential approach (9, 10, 13, 14)). The resulting model is then one-dimensional in the axial direction. Apart from the use of charge regulation, the present model also explicitly takes into account the concentration of protons and hydroxyl ions (i.e., the pH) in the solution (18–20). Sodium chloride is used as a model electrolyte, which can be acidified or alkalized by the addition of HCl or NaOH, respectively. Also mixtures with other univalent and divalent cations are considered. We will confine ourselves to the description of a stationary experiment in a dead-end permeation setup with a constant feed salt concentration (infinitely large feed reservoir), and without any sweep flow on the effluent side. The ion concentrations on the effluent side are not fixed, but are a unique function of the ion and solvent flow through the membrane.

The transport model predicts well-known NF separation characteristics like an increase in retention with increasing pressure difference as well as negative retentions for multicomponent electrolyte mixtures. Other interesting features of the model are nonequal anion and cation retentions at high and low pH values, as well as an optimum pore size for retention at a fixed pressure difference over the membrane.

THEORY

We will consider a membrane consisting of long and narrow straight cylindrical pores of equal length extending from the feed side to the effluent side and focus on a single pore, see Fig. 1. The solution at the left side of the pore is the feed solution; the solution on the right side is the effluent. For long enough pores entrance and exit effects can be neglected. Furthermore, if the pore is narrow enough the ionic concentrations and electrostatic potential are constant with respect to the pore radius, allowing us to neglect radial effects and use a purely one-dimensional description of flow. This approach is referred to as the uniform potential (UP) approach (9, 10, 13, 14).

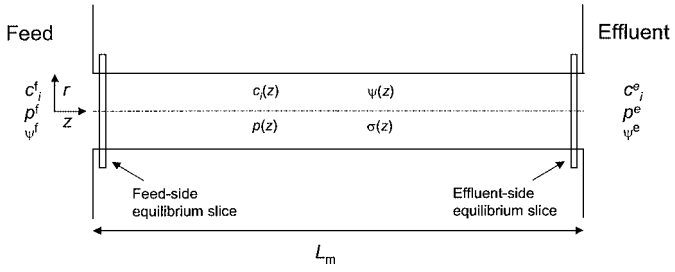

FIG. 1. Overview of a cylindrical membrane pore.

On the feed side of the pore the pressure p^{f} [Pa], electrostatic potential ϕ^{f} [V] and the concentrations of species i, c_i^{f} [mol/m^3], are fixed as well as the pressure on the effluent side p^{e}. The ion concentrations c_i^{e} and electrostatic potential ϕ^{e} in the effluent are variables in the model and not known a priori. At stationary conditions and without a sweep flow on the effluent side, the concentrations in the effluent are related to the molar flux of ions N_i [mol/m^2 s] and the mass-average velocity v [m/s] by (1, 13, 14, 18, 20)

$$c_i^{\mathrm{e}} = \frac{N_i}{v}. \qquad [1]$$

In this work the variables N_i and v are quantities averaged over the pore radius. Since we only consider dilute systems the mass-average velocity is set equal to the solvent velocity.

The pore slices at each end of the membrane are assumed to be in thermodynamic equilibrium with the adjacent solution phases, feed, or effluent. This implies that at the solution-pore interfaces the Boltzmann equation (Eq. [4]) can be used (e.g., 2, 8). All nonequilibrium aspects (i.e., transport) are considered to depend only on the characteristics of the pore in between the two equilibrium slices. Between these equilibrium slices the Boltzmann equation is replaced by the Nernst-Planck equation (Eq. [13]).

For stationary conditions, continuity of mass results in

$$\frac{dN_i}{dz} = 0, \quad \frac{dv}{dz} = 0, \qquad [2]$$

with z the axial coordinate. Hence, N_i and v are constant everywhere in the pore.

When the molar fluxes N_i of ions and the solvent velocity v are known, the effluent concentrations can be obtained from Eq. [1]. The retention by the membrane of each ion species i is

then given by

$$R_i = \left(1 - \frac{c_i^{\mathrm{e}}}{c_i^{\mathrm{f}}}\right) \cdot 100\%. \quad [3]$$

1. Thermodynamic Equilibrium

For dilute, ideal systems at thermodynamic equilibrium the Boltzmann equation relates ion concentrations c_i [mol/m^3] to the electrostatic potential

$$c_i^0 = c_i^{\mathrm{b}} \exp[-z_i(\psi^0 - \psi^{\mathrm{b}})], \quad [4]$$

with z_i the charge number of species i, ψ the dimensionless potential $\psi = F\phi/RT$, with ϕ the electrostatic potential [V], F the Faraday constant [C/mol], R the gas constant [J/(mol · K)], and T the temperature [K]. Here we have written the Boltzmann equation for the equilibrium between a bulk (b) solution (being the feed, f, or the effluent, e), and the solution phase just inside the pore (0). In the feed solution we set the dimensionless electrostatic potential ψ^{f} to zero, but the potential in the effluent ψ^{e} is not fixed.

For electric field strengths higher than ≈20 MV/m, hydration of ions may be important and this effect can be incorporated in Eq. [4] (3, 11).

2. Charge Regulation

Ionic species present in the pore solution adsorb on the membrane pore wall resulting in the formation of a surface charge according to the principles of charge regulation. When several different ionic species are present, competition for the fixed number of surface sites, called competitive adsorption, takes place. In this work we assume an oxidic surface with a fixed number of hydroxyl sites $[-\mathrm{OH}]^{\mathrm{s}}$ (18–23, 27). These surface sites are in thermodynamic equilibrium with the protons (formally, H_3O^+) in the solution next to the surface that may adsorb or desorb at the surface, resulting in $[-\mathrm{OH}_2^+]^{\mathrm{s}}$ or $[-\mathrm{O}^-]^{\mathrm{s}}$ surface groups. Cations and anions adsorb on these negative and positive surface groups, respectively. This adsorption approach is termed the 2-pK model.

An oxidic material can be characterized in terms of the total fixed number of chargeable hydroxyl groups on the membrane pore wall, $c_{\mathrm{tot}}^{\mathrm{s}}$ [mol/m^2], the isoelectric point, which is the pH at which the number of positively and negatively charged surface groups on the material is equal, and $\Delta \mathrm{p}K$, the difference between $\mathrm{p}K^+$ and $\mathrm{p}K^-$ (24–26). The parameters $\mathrm{p}K^+$ and $\mathrm{p}K^-$ describe the equilibrium between the uncharged surface hydroxyl group $[-\mathrm{OH}]^{\mathrm{s}}$ and the charged groups $[-\mathrm{O}^-]^{\mathrm{s}}$ and $[-\mathrm{OH}_2^+]^{\mathrm{s}}$. They are related to the pH at the isoelectric point by

$$\mathrm{pH}_{\mathrm{IEP}} = \frac{1}{2}(pK^+ + pK^-). \quad [5]$$

In this paper we assume that cations $\mathrm{C}^{\mathrm{n}+}$ and anions $\mathrm{A}^{\mathrm{m}-}$ adsorb only on a single charged surface group, irrespective of the ion valency, forming either $[-\mathrm{O}^-\mathrm{C}^{\mathrm{n}+}]^{\mathrm{s}}$ (adsorption constant K_C) or $[-\mathrm{OH}_2^+\mathrm{A}^{m-}]^{\mathrm{s}}$ groups (K_A). Note that only for monovalent cations, C^{1+}, and monovalent anions A^{1-}, these ion pairs are neutral, while for a divalent cation like Ca^{2+}, the adsorbed complex has a 1+ charge. More complex surface adsorption reactions (27) can be built into the charge regulation model as well as the strong adsorption of specifically adsorbing divalent ions (30, 31). However, the 2-pK model used here describes the main features of competitive ion adsorption and charge regulation.

The four surface reactions we will consider are

$$-\mathrm{OH}_2^+ \overset{K^+}{\rightleftharpoons} -\mathrm{OH} + \mathrm{H}^+(\mathrm{s})$$

$$-\mathrm{OH} \overset{K^-}{\rightleftharpoons} -\mathrm{O}^- + \mathrm{H}^+(\mathrm{s})$$

$$-\mathrm{O}^-\mathrm{C}^{\mathrm{n}+} \overset{K_C}{\rightleftharpoons} -\mathrm{O}^- + \mathrm{C}^{\mathrm{n}+}(\mathrm{s})$$

$$-\mathrm{OH}_2^+\mathrm{A}^{\mathrm{m}-} \overset{K_A}{\rightleftharpoons} -\mathrm{OH}_2^+ + \mathrm{A}^{\mathrm{m}-}(\mathrm{s}),$$

where $\mathrm{H}^+(\mathrm{s})$, $\mathrm{C}^{\mathrm{n}+}(\mathrm{s})$, and $\mathrm{A}^{\mathrm{m}-}(\mathrm{s})$ are the proton, cation, and anion in the solution next to the surface, respectively. The equilibrium constants K for these four reactions are defined as

$$K^+ = \frac{c_{\mathrm{H}}^{\mathrm{s}}[-\mathrm{OH}]^{\mathrm{s}}}{c^{\mathrm{ref}}[-\mathrm{OH}_2^+]^{\mathrm{s}}}, \quad K^- = \frac{c_{\mathrm{H}}^{\mathrm{s}}[-\mathrm{O}^-]^{\mathrm{s}}}{c^{\mathrm{ref}}[-\mathrm{OH}]^{\mathrm{s}}},$$
$$K_C = \frac{c_{\mathrm{C}}^{\mathrm{s}}[-\mathrm{O}^-]^{\mathrm{s}}}{c^{\mathrm{ref}}[-\mathrm{O}^-\mathrm{C}^{\mathrm{n}+}]^{\mathrm{s}}}, \quad K_A = \frac{c_{\mathrm{A}}^{\mathrm{s}}[-\mathrm{OH}_2^+]^{\mathrm{s}}}{c^{\mathrm{ref}}[-\mathrm{OH}_2^+A^{\mathrm{m}-}]^{\mathrm{s}}}. \quad [6]$$

The concentrations of the surface complexes ($[-\mathrm{OH}]^{\mathrm{s}}$, $[-\mathrm{OH}_2^+]^{\mathrm{s}}$, $[-\mathrm{O}^-]^{\mathrm{s}}$, $[-\mathrm{O}^-\mathrm{C}^{\mathrm{n}+}]^{\mathrm{s}}$, $[-\mathrm{OH}_2^+\mathrm{A}^{\mathrm{m}-}]^{\mathrm{s}}$) have units [mol/m^2], the ion concentrations in the pore solution next to the surface c_i^{s} have units [mol/m^3], and c^{ref} is the thermodynamic reference concentration ($c^{\mathrm{ref}} = 1000$ mol/m^3, corresponding to 1 mol/dm^3). The adsorption equilibrium constants K^+, K^-, K_A, K_C, and $c_{\mathrm{tot}}^{\mathrm{s}}$ describe the interaction of the (membrane) material with the respective ion and the solvent for the given adsorption model and are independent of such factors as pore size, geometry, pH, and ion concentration. Because they are material specific, they can be determined independently by techniques like electrophoretic mobility measurements or electroacoustic methods.

The surface charge σ [C/m^2] is given by

$$\sigma = F\left([-\mathrm{OH}_2^+]^{\mathrm{s}} - [-\mathrm{O}^-]^{\mathrm{s}} + \sum_{i=1}^{nC}(n_i - 1)\left[-\mathrm{O}^-\mathrm{C}_i^{\mathrm{n}_i+}\right]^{\mathrm{s}} - \sum_{i=1}^{nA}(m_i - 1)\left[-\mathrm{OH}_2^+\mathrm{A}_i^{\mathrm{m}_i-}\right]^{\mathrm{s}}\right), \quad [7]$$

with nC and nA the total number of cation and anion species,

respectively. The total number of surface sites c^s_{tot} [mol/m^2] is equal to the sum over all surface sites,

$$c^s_{tot} = [-OH]^s + [-OH_2^+]^s + [-O^-]^s + \sum_{i=1}^{nC}\left[-O^-C_i^{n_i+}\right]^s + \sum_{i=1}^{nA}\left[-OH_2^+A_i^{m_i-}\right]^s. \quad [8]$$

Combining Eqs. [7] and [8] with the adsorption reactions in Eq. [6] results in a surface charge given by

$$\sigma = Fc^s_{tot}\frac{\frac{c^s_H}{K^+}\left[1-\sum_{i=1}^{nA}(m_i-1)\frac{c^s_{A,i}}{K_{A,i}}\right]-\frac{K^-}{c^s_H}\left[1-\sum_{i=1}^{nC}(n_i-1)\frac{c^s_{A,i}}{K_{C,i}}\right]}{1+\frac{c^s_H}{K^+}\left(1+\sum_{i=1}^{nA}\frac{c^s_{A,i}}{K_{A,i}}\right)+\frac{K^-}{c^s_H}\left(1+\sum_{i=1}^{nC}\frac{c^s_{A,i}}{K_{C,i}}\right)}. \quad [9]$$

In case of only one type of monovalent anion and one type of monovalent cation, Eq. [9] results in a surface charge given by (3, 21, 23, 36)

$$\sigma = Fc^s_{tot}\frac{\left(c^s_H\right)^2 - K^+K^-}{K^+c^s_H + \left(c^s_H\right)^2 + K^+K^- + K^+K^-c^s_C/K_C + \left(c^s_H\right)^2 c^s_A/K_A}. \quad [10]$$

In some of the simulations we will use the divalent calcium ion as well. With the assumption that this ion only adsorbs at one single $[-O^-]^s$ site, the surface charge can be calculated with Eq. [9] ($nA = 1, nC = 2$).

In the model, the surface charge is calculated at every axial position in the membrane and is supplemented by another expression for the surface charge resulting from the constraint of electroneutrality in each pore slice.

3. Electroneutrality

In every pore slice the sum of the mobile charges (the charges related to the ions in the pore solution) is assumed compensated by the immobile charge on the pore surface. Hence, the surface charge σ [C/m^2] is given by

$$\sigma(z) = -\frac{1}{a}\int_0^a F\sum_{i=1}^{ni} z_i c_i(z,r) r\, dr, \quad [11]$$

with ni the number of ionic species ($ni = nA + nC$), a the pore radius [m], r the radial coordinate [m], and c_i a function of z and r. In the uniform potential model (9, 10, 13, 14) the concentrations are constant over the radial coordinate (see Fig. 1), and Eq. [11] becomes

$$\sigma(z) = -\frac{Fa}{2}\sum_{i=1}^{ni} z_i c_i(z). \quad [12]$$

4. The Nernst-Planck Equation

The Nernst-Planck equation can be derived from the full Maxwell-Stephan equation for dilute, ideal systems (17) and is given by

$$N_i = -D_i\left(\frac{dc_i}{dz} + z_i c_i\frac{d\psi}{dz}\right) + c_i v. \quad [13]$$

The diffusion coefficients D_i [m^2/s] are equal to the Maxwell-Stefan ion-solvent diffusion coefficients at infinite dilution (17). The constraints of the porous membrane matrix hinder transport, and the diffusion coefficients as well as the convective velocity can be adjusted to account for these geometrical effects (11, 14, 32, 33). For example, Bowen *et al.* (12) use a correction from the theory of hydrodynamics for both diffusion and convection. Another particular elegant manner to include matrix effects—hindered transport of both solvent and ions—is the inclusion of the Einstein correction, simultaneously in the diffusion coefficient D_i (Eq. [13]) as well as in the viscosity μ (Eq. [15]). This approach was used by Yang and Pintauro (11) and allowed them to quantitatively describe membrane retention data (their Fig. 3). In the present paper we will not apply such corrections and assume that transport by diffusion and convection in the membrane pore is equal to transport in free solution.

In principle, the Nernst-Planck equations should be solved for all charged mobile species (hydroxyl ions, protons, anions, and cations). However, for the hydroxyl ions we apply the water dissociation reaction instead, which is fast compared to the transport processes. The water dissociation reaction is given by

$$K_w = c_{H^+}c_{OH^-}, \quad [14]$$

where K_w is the water autoprotolysis constant [mol^2/m^6]. Contrary to (18–20) we assume Eq. [14] to be valid at each location in the membrane. Because the molar fluxes are related to the effluent concentrations by Eq. [1], the flux of hydroxyl ions follows directly from the flux and the effluent concentration of protons (Eq. [14]).

5. The Navier-Stokes Equation

Solving the full Navier-Stokes (NS) equation is a formidable task. We will therefore limit ourselves to systems with a constant mass density and viscosity. Neglecting radial velocities v_r and pressure gradients $\partial p/\partial r$ and using the uniform potential approach, we only have to consider the axial component of the NS equation. At mechanical equilibrium, with cylindrical symmetry (i.e., $\partial/\partial\theta = 0$) and zero tangential velocity, the axial component of the NS equation reads

$$-\frac{dp}{dz} + \mu\left[\frac{1}{r}\frac{\partial}{\partial r}\left(r\frac{\partial v_z}{\partial r}\right) + \frac{\partial^2 v_z}{\partial z^2}\right] - RT\sum_{i=1}^{ni} z_i c_i\frac{d\psi}{dz} = 0, \quad [15]$$

with p the pressure [Pa] and μ the Newtonian viscosity [Pa · s]. Integrating Eq. [15] twice subject to the boundary conditions

$$\left.\frac{\partial v_z}{\partial r}\right|_{r=0} = 0 \qquad v_z|_{r=a} = 0, \qquad [16]$$

and using Eq. [2] results in

$$v_z(r) = \frac{a^2}{4\mu}\left[1 - \left(\frac{r}{a}\right)^2\right]\left(\frac{dp}{dz} + RT\sum_{i=1}^{ni} z_i c_i \frac{d\psi}{dz}\right). \qquad [17]$$

Integrating over the pore radius a, the average velocity v is obtained (9)

$$v = -\frac{a^2}{8\mu}\left(\frac{dp}{dz} + RT\sum_{i=1}^{ni} z_i c_i \frac{d\psi}{dz}\right). \qquad [18]$$

If the electrostatic term in Eq. [18] is neglected the classical parabolic Hagen-Poiseuille flow profile is obtained (34), but the expression shows that also for the uniform potential approach the flow profile is always parabolic.

Instead of the pore-ensemble approach it is also possible to model a membrane as a porous packed bed. In this concept the permeability of the material κ [m^2] replaces $a^2/8$ in Eq. [18] (34, 35). The permeability depends on the porosity, the tortuosity, and the size of the particles of which the porous medium consists. In the present paper, however, Eq. [18] is used instead.

6. *Zero Electric Current*

Charged mobile species of opposite sign cannot move through the membrane independently since even minute amounts of charge separation will give rise to very large electrostatic fields. These fields will immediately adjust the ion molar fluxes to obtain a zero electric current,

$$F\sum_{i=1}^{ni} z_i N_i = 0. \qquad [19]$$

7. *Uniform Potential Assumption*

In our model only transport through narrow pores is considered. As a result, gradients in the radial concentrations and radial electrostatic potential can be neglected; this is the uniform potential approach (9, 10, 13, 14). Indeed, this assumption becomes increasingly exact when equally charged opposing surfaces approach each other (36). To assess the validity of this assumption for our system of cylindrical pores, and to select a proper base case, we calculated the radial concentration and electrostatic potential profile using the exact Poisson-Boltzmann equation for a system consisting of monovalent ions only,

$$\frac{\lambda^2}{\rho}\frac{d}{d\rho}\left(\rho\frac{d\psi}{d\rho}\right) = \sinh(\psi). \qquad [20]$$

The Debye ratio λ is the ratio of the Debye length λ_D over the pore radius a, $\lambda = a^{-1}\sqrt{\varepsilon_r\varepsilon_0 RT \cdot (2F^2c^f)^{-1}}$, with c^f the ionic strength, and ρ the dimensionless radial coordinate, $\rho = ra^{-1}$.

Figure 2a shows the deviation between the concentration at the pore surface and at the pore centerline for a monovalent salt as a

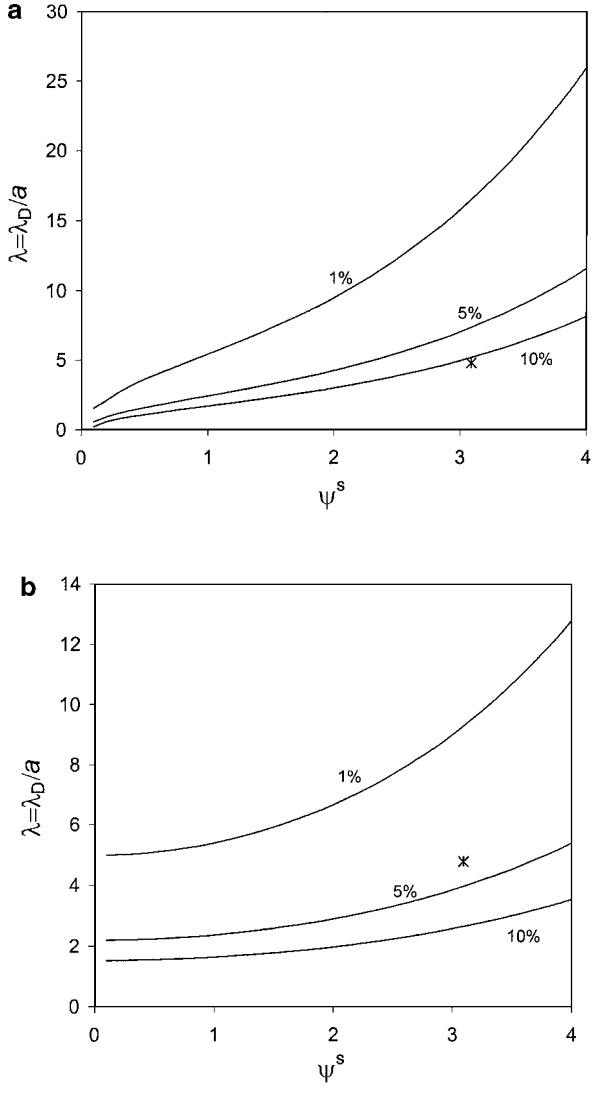

FIG. 2. Deviation from the uniform potential approach as a function of the dimensionless surface potential ψ^s and λ (λ is the ratio of the Debye-length and the pore radius) calculated using the exact Poisson-Boltzmann equation for a monovalent symmetrical electrolyte. The star is the base case. (a) Deviation in cation concentration between the pore center ($r = 0$) and the pore wall ($r = a$). (b) Deviation in electrostatic potential between the pore center and the pore wall.

TABLE 1
Data Used in the Simulations

$c_{s,tot} = 8.3 \times 10^{-6}$ mol/m^2 which follows from 20 Å^2 per site (25)
$\Delta pK = pK^- - pK^+ = 3$ (25), $pH_{IEP} = 9.25$ (alumina)
thus $K^- = 1.778 \times 10^{-11}$ and $K^+ = 1.778 \times 10^{-8}$
$K_A = K_C = 7.0 \times 10^{-5}$
Pore size $(2a) = 4$ nm and membrane thickness (pore length) $L_m = 1$ μm
$K_w = 1 \times 10^{-8}$ mol^2/m^6
$D_{H^+} = 9.31 \times 10^{-9}$, $D_{Na^+} = 1.33 \cdot 10^{-9}$, $D_{Cl^-} = 2.03 \times 10^{-9}$,
$D_{Ca^+} = 0.79 \times 10^{-9}$ m^2/s (47)
For the feed solution $c^f = 1$ mol/m^3, $pH^f = 6$
$\mu = 8.85 \times 10^{-4}$ Pa · s, $p^f - p^e = 0.5$ MPa
$F = 96485$ C/mol, $R = 8.3144$ J/(mol · K), $T = 298.15$ K
$\varepsilon_r = 78$, $\varepsilon_0 = 8.854 \cdot 10^{-12}$ C/(V · m)

function of the dimensionless surface potential ψ^s and the Debye ratio λ while Fig. 2b shows the deviation in electrostatic potential in the center of the pore ψ^0 from its value at the surface ψ^s. Bowen *et al.* (14) made a similar assessment for the applicability of the uniform potential approach.

When the radial potential distribution was obtained from Eq. [20] the concentration profile was calculated using Eq. [4] (setting the electrostatic potential in the feed to zero). Analyzing Fig. 2a and Fig. 2b shows that for dimensionless surface potentials ψ^s below 1.0 ($\phi^s < 25.7$ mV) the deviation in the radial ion concentration is lower than the deviation in radial potential, while the opposite is true for $\psi^s > 1.0$.

To select a proper base case (Table 1), we combined Eq. [20] with the charge regulation expression (Eq. [10]) and the electroneutrality condition (Eq. [12]). For our base case a deviation in the concentration of approximately 10% was considered acceptable and the base case was selected accordingly (the single star in Fig. 2a and Fig. 2b shows the position of the base case).

8. Solution Scheme

The 1D transport model consists of a coupled set of $3ni + 5$ differential and algebraic equations (ni is the number of ionic species) which is simultaneously solved for the independent variables: the molar fluxes N_i, the solvent velocity v, the effluent concentrations c_i^e, and the dimensionless potential in the effluent ψ^e (all independent of z), the concentrations of species i, $c_i(z)$, the dimensionless axial potential gradient, $(d\psi/dz)(z)$, the pressure, $p(z)$, and the membrane surface charge $\sigma(z)$ (all a function of the axial coordinate z). The feed concentrations c_i^f are known a priori as well as the pressures in both solution phases.

Because of thermodynamic equilibrium, the concentrations and potential in the pore at the left equilibrium slice can be calculated using Eqs. [4] (we define a reference potential by setting the potential in the feed to zero), [10], [12], and [14]. The ion concentrations in the effluent c_i^e are variables in the model and therefore not known a priori, but are related to the ion fluxes and solvent velocity by Eq. [1]. In between the equilibrium slices in the membrane the Nernst-Planck equation [13] is solved for each of the ionic species as well as the integrated Navier–Stokes equation [18] and charge regulation relations [10] at each pore slice under the conditions of electroneutrality [12] and zero electric current [19].

The system of equations [10], [12], [13], and [18] is discretized and written in a finite difference scheme, resulting in a set of "pore slices," while Eqs. [1] and [19] are only solved once, independent of the number of pore slices in the model.

The unknown parameters are then calculated with a Newton-Raphson iteration procedure. Before implementation, numerical stability was checked by testing different finite discretization schemes and changing the number of grid points. The complete model is implemented in the mathematical program Maple (Waterloo Maple, Ontario, Canada).

RESULTS AND DISCUSSION

1. Base Case

Model results will be discussed using a base case for which we consider a pore radius a of 2 nm. The feed solution contains 1 mol/m^3 NaCl at a pH of 6, obtained by the addition of HCl (for pH > 7, NaOH is added). The applied pressure difference over the membrane is 0.5 MPa. We consider a γ-alumina membrane and use the material parameters given in Table 1.

For the base case, the deviation from the uniform potential model assumption is 11.6% for the radial cation concentration, 3.8% for the electrostatic potential, and 3.1% for the surface charge (see section 7 under Theory). In all other simulations, the deviation in the radial concentration was smaller than 11.6% unless otherwise specified (see Fig. 9b).

2. Limiting Retention

It is well known from practice that at increasing pressure differences the retention increases but reaches a limiting retention at very high pressures (11, 37–39); the charge regulation model also predicts this phenomenon (Fig. 3). The initial increase in retention for increasing pressure differences is a result of the fact that water transport is enhanced more than ion transport: the velocity of water is almost proportional to the pressure difference (see Fig. 2 in Ref. (38) as well as Eq. [18], the component with the axial potential gradient is in general very small), while transport of ions is reduced by migration (due to the axial electric field that originates from the condition of zero electrical current). For ever increasing pressure differences, however, convection becomes the most important transport mechanism for both water and ions, finally resulting in the limiting retention.

In a previous paper (21), we modeled the retention of a hydrophilic membrane applying the CR model to a cylindrical pore slice, far enough from either of the pore interfaces for axial concentration gradients to be zero, and in thermodynamic equilibrium with the feed solution. (Accidentally, in (21) the words co-ion and counterion were switched in Eq. [13]. The coions

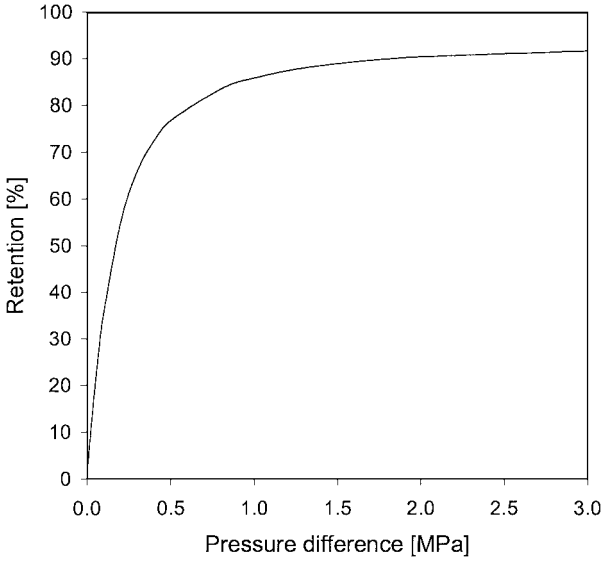

FIG. 3. Anion and cation retention (equal) as a function of pressure difference. Base case conditions of Table 1 (NaCl + HCl) except for the pressure.

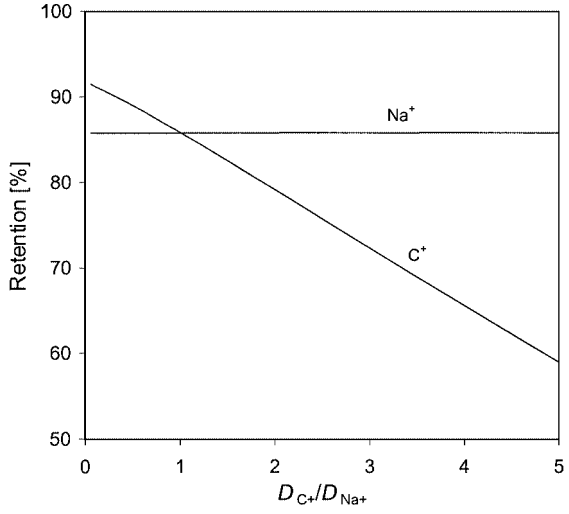

FIG. 5. Retention of sodium and another cation C^+ as a function of the diffusion coefficient of C^+ for a mixture of 1 mol/m^3 NaCl and 1 mol/m^3 CCl, pH 6. Base case conditions of Table 1.

are the ions that are excluded from the membrane (same charge as the membrane), while the counterions are the ions present in excess in the pores (opposite charge)). In Fig. 4 we compare the cation retention predicted with the equilibrium model (21) with the results from the present model incorporating transport. The models coincide only at very low values of the cation diffusion coefficient. This is because for small enough diffusion coefficients, the cation (the co-ion in a positively charged membrane) will be "frozen" in the solvent flow, moving at the same velocity as the solvent; in a binary electrolyte the counterions are then forced to move with the same molar flux as the co-ions because of the zero-current condition. For negatively charged membranes, the anion is the co-ion and we expect the transport model to approach the equilibrium model (21) for very low anion diffusion coefficients.

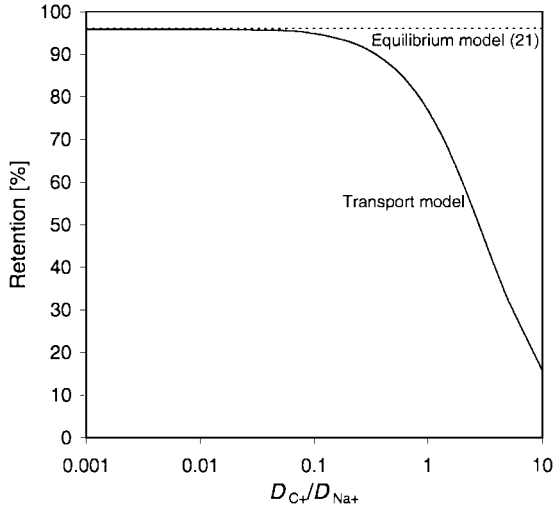

FIG. 4. Anion and cation retention (equal) as a function of the diffusion coefficient of the cation, C^+, for the equilibrium model ((21), dotted line) and the transport model (solid line). Base case conditions of Table 1.

3. Influence of Mobility and Charge on Retention

In Fig. 5 we show the effect on retention when instead of one co-ion, two co-ions with different mobilities (diffusion coefficients) are present in the solution. In the simulation a mixture of NaCl and CCl (C^+ being an undefined monovalent cation) of equal molarity is considered. Similar to the observations in Fig. 4, a lower cation mobility (of C^+ compared to Na^+) results in a higher retention for C^+. The reverse effect occurs at mobilities of C^+ higher than that for Na^+. For a very high mobility of C^+, the model even predicts negative retentions for C^+ but this occurs only at an unrealistically large value of D_{C^+}/D_{Na^+} (not shown).

Yaroshchuk *et al.* (40) and Bardot *et al.* (41) measured retentions in multicomponent mixtures (Cs + Li, Cs + Na + Li, Cs + Na, and K + Li) on negatively charged membranes and obtained decreasing retentions for cations with decreasing mobility in the order Cs > Na/K > Li. In mixtures of Li^+ with Cs^+ or K^+, negative retentions for lithium could be found. Interestingly, this experimental behavior seems exactly opposite to what our model predicts, namely that the less mobile cations are better retained. However, Yaroshchuk *et al.* (40) and Bardot *et al.* (41) measured retentions on a negatively charged membrane, while the membrane considered in Fig. 5 is positively charged. Hence, where in our calculations the positive ions are the co-ions, in (37, 41) they are the counterions, which reverses the retention-mobility behavior of the cations: in positive membranes a reduced mobility of cations increases the retention while in a negative membrane a reduced mobility of cations decreases

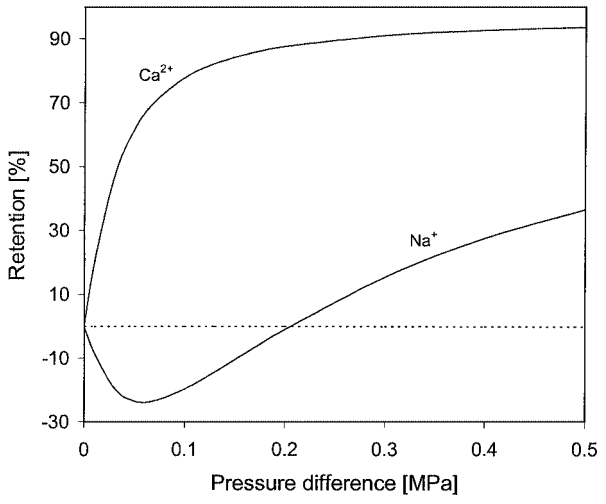

FIG. 6. Retention for calcium and sodium ions as a function of pressure in a mixture of 1 mol/m^3 $CaCl_2$ and 1 mol/m^3 NaCl, pH 6. Base case conditions of Table 1 except for the pressure difference and concentrations.

the retention, see also (37). Simulations at a pH of 11, where our system becomes negatively charged, indeed showed a decreasing retention with decreasing cation mobility (simulations not reported), confirming that our model results are in qualitative agreement with the experimental results in (40, 41).

Retention depends not only on ion mobility but also on ion charge. Indeed, negative retentions have been found experimentally for mixtures of ions with different valencies (1, 37). We show in Fig. 6 that the present charge regulation model also predicts this effect. In the simulations for Fig. 6 we added 1 mol/m^3 calcium chloride to a solution of sodium chloride of the same molarity (pH = 6). The adsorption equilibrium constants of sodium and calcium in the charge regulation relation (Eq. [9]) were arbitrarily set equal (i.e., $K_{Na^+} = K_{Ca^{2+}} = 7 \times 10^{-5}$). Calcium is retained much better than sodium, and negative retentions are found for sodium for low pressure differences (i.e., low solvent velocities). The origin of the higher retention for calcium lies mainly in its higher charge number: it is more effectively excluded from the pores by the positive electrostatic potential, Eq. [4], which is due to the positive surface charge on the membrane. Note that this behavior only occurs for positively charged membranes. For negatively charged membranes, the retention of divalent cations is lower than the retention for monovalent cations, for binary electrolytes with the same anion.

4. Retention as Function of pH

The predictive power of the charge regulation model is clearly shown in Fig. 7a where the retention is shown as function of the pH in the feed solution. In the pH range commonly used in experimental work (pH 6–7) the retentions of anions and cations are equal. This is because the concentrations of hydroxyl ions and protons (H_3O^+) are very low and almost equal. For pH values lower than 4 and higher than 10 the anion and cation retentions clearly start to deviate. The deviation in cation and anion retentions at low and high pH is a result of the fact that we have incorporated transport of protons and hydroxyl ions in the model. At decreasing pH the proton concentration in the system increases and the protons start to influence the retention of the other ions: in the pore and effluent the slow cations (low mobility) are replaced by the much faster protons, causing the higher retention of cations compared to those of the anions (see Fig. 5). At pH values above the IEP the situation is reversed: the hydroxyl ions replace the much slower anions, increasing the retention of the latter (18, 19). When the feed salt concentration is increased, the influence of hydroxyl ions and protons is reduced and more extreme pH values are required to observe the diverging retention of cations and anions (Fig. 7b).

Apart from the influence of protons and hydroxyl ions (pH), the retention of ions depends also on the surface charge. This is

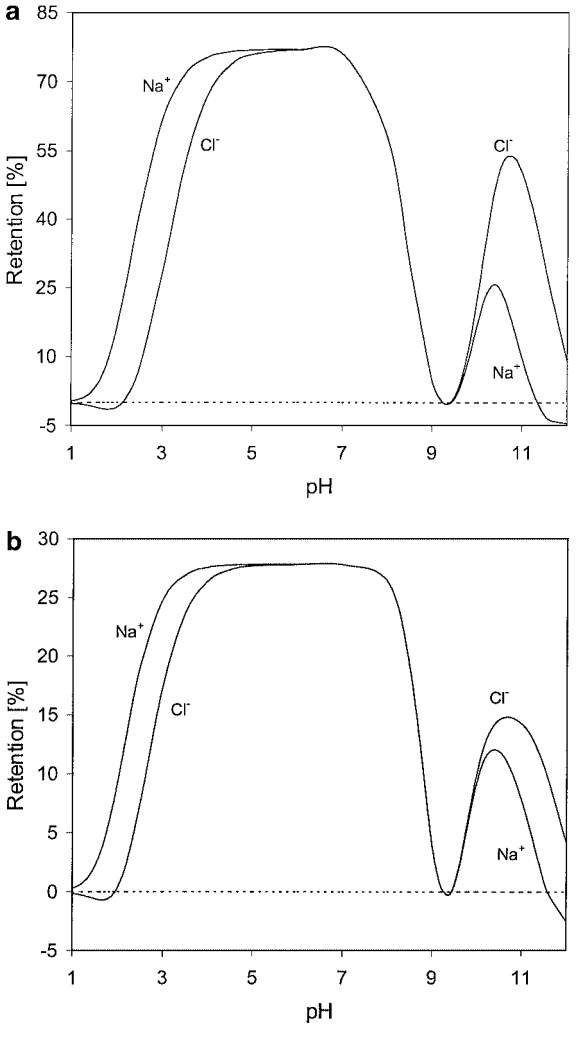

FIG. 7. Anion and cation retention as a function of pH. Base case conditions of Table 1 (NaCl + HCl) except for the pH. (a) 1 mol/m^3 NaCl, (b) 5 mol/m^3 NaCl.

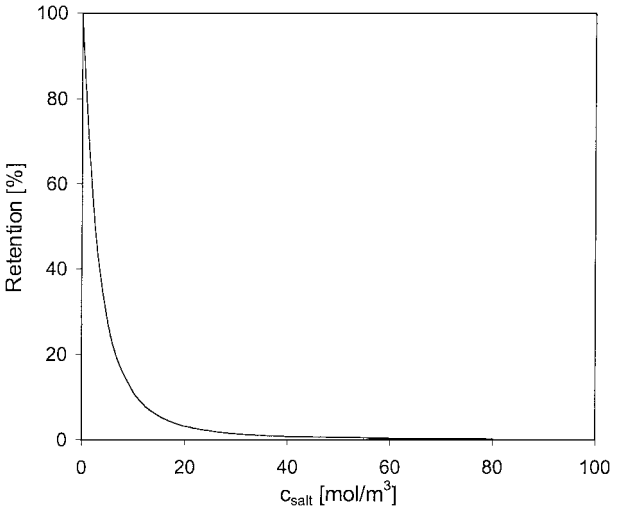

FIG. 8. Anion and cation retention (equal) as a function of the electrolyte concentration in the feed. Base case conditions of Table 1 (NaCl + HCl) except for the feed solution concentration.

most clearly observed at the isoelectric point of the membrane ($pH_{IEP} = 9.25$; Fig. 7a). Because the effective membrane surface charge is zero at the IEP, a zero retention is predicted; see (21) as well.

5. *Retention as Function of Feed Salt Concentration*

The CR model predicts that increasing the feed electrolyte concentration will result in a decreasing retention, see Fig. 8 and (21). The reason is the reduced surface charge and electrostatic potential in the pore at increasing feed concentrations. As a result, the concentrations of co-ions and counterions in the pore become more equal to each other and to the feed concentration, leading to higher ion fluxes and therefore lower retentions (see Eq. [1]). Although this behavior is experimentally found for some (inorganic) materials (37–39) it does not seem to apply as a rule (42).

6. *Retention as Function of Pore Size*

When the pore size of a membrane is reduced the retention will increase (19, 37, 39). This behavior is shown in Fig. 9a for a constant solvent velocity v. To obtain a constant solvent velocity, the decrease in pore size must be counterbalanced by an increase in the pressure difference, see Eq. [18]. For such cases the retention always increases continuously with decreasing pore size. However, when the pressure difference $p^e - p^f$ is kept constant and the pore size is varied (Fig. 9b) the retention behavior is completely different: the retention increases with increasing pore size for most cases considered. For very high pressures of 2 MPa the retention attains a maximum for a pore size of 5.5 nm (optimum pore size). In Fig. 9b the optimum pore size is difficult to distinguish and occurs only at high deviations from the uniform potential model (≈20% deviation). In other simulations (not reported) with lower diffusion coefficients, the optimum in pore size occurs at a lower pore size, within the 10% deviation limit, and is much more pronounced.

We examined the influence of pH and feed salt concentration on the location of the optimum pore size. There were only small effects for both parameters. The (constant) pressure difference that we considered, however, had a profound influence on the position of the optimum. For increasing pressure differences, the optimum in pore size shifted to lower values though the effect levels off at higher pressure differences (see Fig. 9b). The finding in Fig. 9b is quite remarkable, but understandable as well. A decreasing pore size will cause the double layers to overlap more, thereby excluding more co-ions from the pore but admitting more counterions. Hence, the co-ion concentration in the pore decreases and the concentration of counterions increases, which increases retention. This effect levels off for decreasing

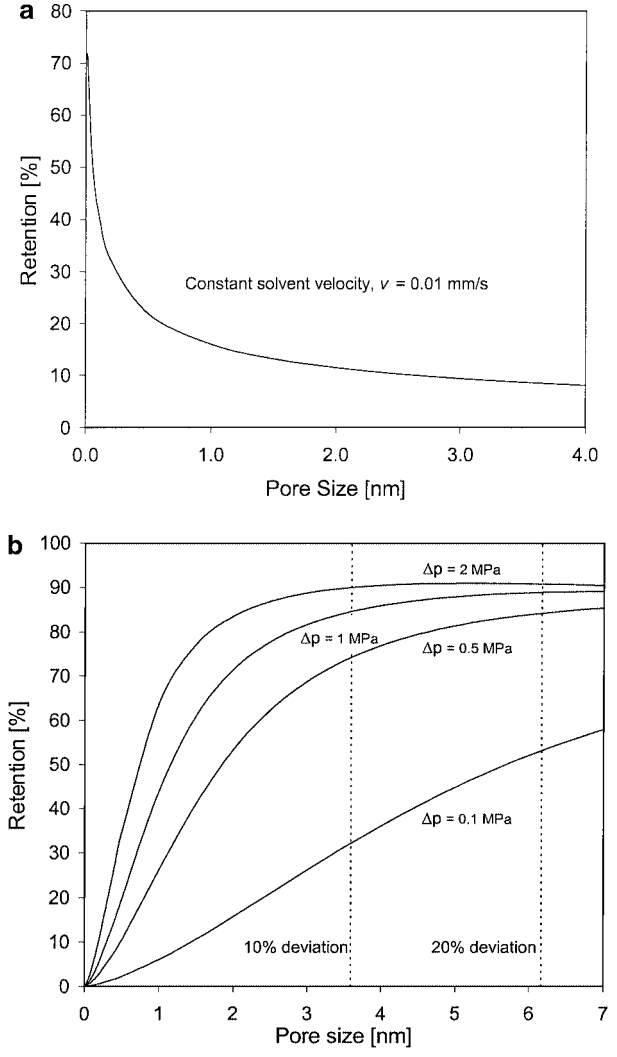

FIG. 9. Anion and cation retention (equal) as function of pore size. Base case conditions of Table 1 (NaCl + HCl) except for the pore radius. (a) Constant solvent velocity of 0.01 mm/s. (b) Constant pressure difference of 0.1, 0.5, 1, and 2 MPa. The dotted lines are the percentage of deviation from the uniform potential assumption.

pore sizes as the double layers become fully overlapped. A second effect of a decreasing pore size is the decrease in solvent velocity, and as was shown in Fig. 3, a decrease in solvent velocity (i.e., a decreasing pressure difference) results in a lower retention. Hence we have two phenomena that counteract each other. Supposedly, with decreasing pore size, the electrostatic exclusion effect becomes important first (before the solvent velocity effect), but is also the first to level off, resulting in an optimum pore size with respect to retention. Unfortunately, no experimental evidence in the literature was found to support the prediction of an optimum pore size for retention.

In other simulations instead of the pore size the pore length L_m was varied, maintaining a constant pressure difference, which showed that the solvent velocity to be inversely proportional to the pore length, as can be expected from Eq. [18]. Interestingly, the ion retention remained constant with varying pore length. This can be explained by the fact that the solvent velocity and the ion molar fluxes decrease to the same extent when the pore length is increased, thereby not influencing the retention, see Eq. [1].

7. Surface Charge

In the present model, the surface charge is calculated at every position in the pore (Fig. 10). However, for the base case of Table 1, the change in surface charge across the membrane is quite small and the use of a constant surface charge (independent of axial coordinate) would not have been of much influence for the prediction of retention and solvent velocity. In such a simplified model, the surface charge is calculated for the left equilibrium slice—only dependent on feed conditions, material properties, and pore size—and this value used for each position in the membrane pore. This simplified approach using a constant surface charge also gives the possibility of fitting the model to experimental retention data to obtain the surface charge of the pores in the membrane (e.g., 1, 13, 14).

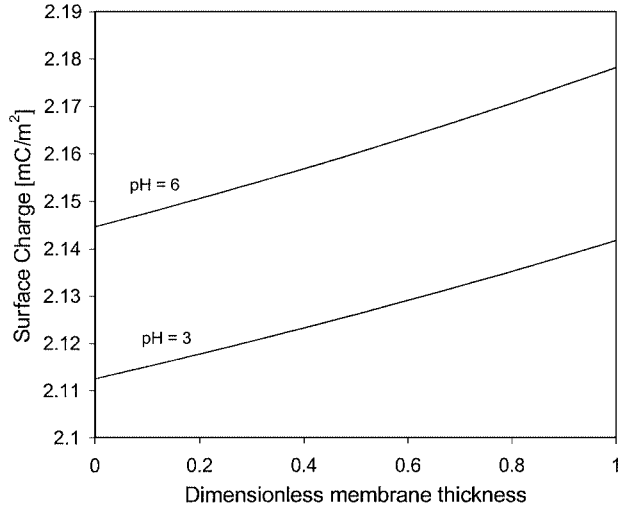

FIG. 10. Surface charge across the membrane (dimensionless thickness: 0, feed side; 1, effluent side). Base case conditions of Table 1 (NaCl + HCl) except for the pH.

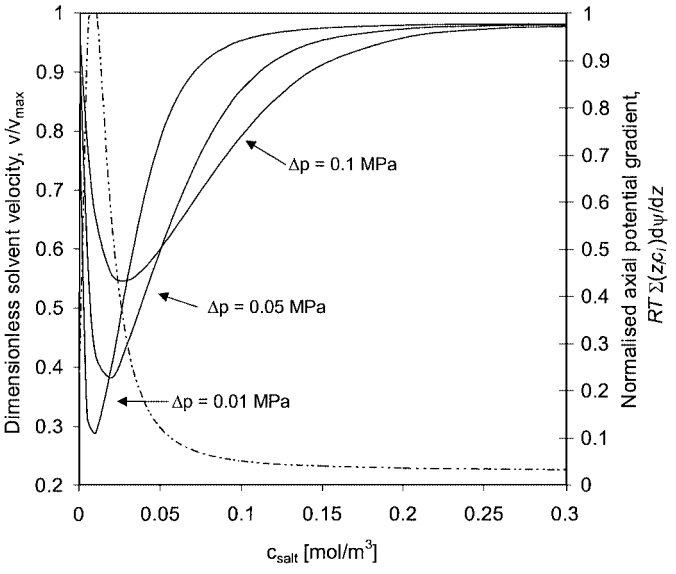

FIG. 11. Dimensionless solvent velocity (solid lines) and normalized axial potential gradient term (dashed line, Eq. [18]) as a function of the feed salt concentration for pressure differences of 0.01, 0.05, and 0.1 MPa. Base case conditions of Table 1 (pH 6) except for the pressure difference and the feed concentration.

Note, however, that the surface charge is a function of all experimental variables (feed salt concentration, feed pH, pore size, etc.) and therefore the surface charge would need to be determined for each new experimental condition. The objective of using the charge regulation boundary condition in this paper is that when the K values and $c_{s,tot}$ have been determined for the membrane material (by some experimental method), surface charge and retention can be predicted a priori when the experimental conditions are changed.

Besides, the surface charge is not always as constant across the membrane as in Fig. 10: for example, in the simulations related to Fig. 11 the surface charge decreased up to 95% across the membrane for salt concentrations of ~30 mmol/m^3. Furthermore, a large change in surface charge will certainly be the case for membranes with changing material properties over the pore length, as is the case for bipolar membranes. Because the surface charge is calculated in each pore slice, the present model would be naturally suited to describe such nonhomogeneous membrane systems.

8. Solvent Velocity

In Fig. 11 the solvent velocity v, as predicted by the charge regulation transport model, is plotted on the left y-axis as function of salt concentration and pressure difference. The solvent velocity is scaled with respect to the maximum solvent velocity at its corresponding pressure difference, v_{max}, which is given by the

Poiseuille equation: Eq. [18] with the (second) electrostatic term omitted. For sufficiently high salt concentrations (>50 mol/m^3; not shown in Fig. 11), v/v_{max} approaches unity because the membrane becomes uncharged and the axial potential gradient vanishes. For a zero salt concentration and at pH 7, $v/v_{max} = 1$ as well, because charge separation is impossible (zero electrical current, and anion and cation concentrations are zero). However, in Fig. 11 simulations were performed at pH = 6 (base case), hence, even for a zero salt concentration v/v_{max} was less than unity.

According to the model, see Fig. 11, the solvent velocity increases linearly with the pressure difference as long as the salt concentration exceeds the (very low) value of ~0.2 mol/m^3. This behavior is well known from experiments, e.g., (38).

The influence of the salt concentration on the solvent velocity v is less straightforward. Starting at $c_{salt} = 0$, with increasing c_{salt}, v first decreases, reaches a minimum around ~10–30 mmol/m^3 after which v increases and levels off. Let us discuss the minimum, the increase in solvent velocity above the minimum, and the leveling-off of the solvent velocity one after the other.

Minimum solvent velocity. The minimum in the solvent velocity predicted by the charge regulation model is caused by the second term between brackets in Eq. [18], $RT \sum_{i=1}^{ni} z_i c_i (d\psi/dz)$. At high salt concentrations the summation over all ions is large but the surface charge is low (see Fig. 8). For small surface charges the electrostatic potential in the pore is low and the co-ion and counterion concentrations approach each other, resulting in a decreasing axial electric field (i.e., $d\psi/dz$ is small). For very low salt concentrations, however, $\sum_{i=1}^{ni} z_i c_i$ is low, but the surface charge and the axial electric field become very large. These phenomena have an opposite effect on $RT \sum_{i=1}^{ni} z_i c_i (d\psi/dz)$, and this term attains a maximum value for very small salt concentrations (see Fig. 11, right y-axis), leading to the observed minimum in the solvent velocity.

Increasing solvent velocity. An increasing solvent velocity with increasing salt concentration is not typically reported in the membrane literature because generally experimental salt concentrations are higher. However, an increase of solvent velocity with salt concentration was recently reported for the flow through the microchannels of pit membranes within xylem vessels in plants (43) for salt concentrations of 0–20 mol/m^3 and especially in the range 0–1 mol/m^3, similar to the increase in solvent velocity predicted by the present model (Fig. 11) up to 0.3 mol/m^3 (dependent on the pressure difference across the membrane).

This qualitative agreement might suggest that the present model that combines electroviscous effects with charge regulation on the pore walls might have relevance for the description of flow through the pit membranes of the xylem vessels in plants. Note that in the experiments (43), a minimum in solvent velocity at a critical salt concentration was not found, perhaps because dissolution of ions from the cell surfaces into the water always increased the salt concentration to above the minimum value.

Decreasing solvent velocity. Contrary to the prediction of the charge regulation model that the solvent velocity approaches the maximum v_{max} with increasing salt concentration, experiments with nanofiltration membranes (39, 42) show a decreasing solvent velocity with increasing feed salt concentration in the range of 1–100 mol/m^3. To understand the reason for this discrepancy, we performed additional simulations.

First, we used a one-dimensional uniform potential model with a constant surface charge from literature (1) and found that it predicts an increase in solvent velocity with salt concentration as well.

Second, we focused our attention on osmotic effects. Indeed, some authors have attributed the decreasing solvent velocity to an increase in the osmotic pressure when the salt concentration increases (28, 42, 44, 45). Others, however, attributed the decrease in solvent velocity only in a minor degree to osmosis but mainly to other effects, such as the degree of dissociated charged groups and a change in the water concentration in the membrane (38). Still, to investigate whether osmosis explains the decrease in solvent velocity, we incorporated osmosis into the charge regulation model by adding to the transport model the term responsible for osmosis, $\bar{V}_i p$, with $\bar{V}_i$ the molar volume [m^3/mol] of species i (46), and we used the full Maxwell–Stefan transport description (17, 33) for the molar fluxes of all mobile species, including water. Unfortunately, in these simulations (not reported), the same result was obtained: the solvent velocity increases with feed salt concentration and levels off, without decreasing at higher salt concentrations. We therefore believe the decreasing solvent velocity with increasing salt concentration (1–100 mmol/m^3 range) in dead-end permeation setups is not related directly to osmotic effects, but must be due to another phenomenon, e.g., a transport resistance leading to concentration polarization outside the membrane. These effects can be incorporated using film models that are well known and available in literature (e.g., 13, 17, 34).

CONCLUSIONS

We combined charge regulation with the relevant transport relations to describe ion retention of and solvent flow through a charged nanofiltration membrane consisting of cylindrical capillaries. For the base case with a pore size of 4 nm, the deviation from the uniform potential assumption was 11.6% for the cation concentration and 3.8% for the electrostatic potential. The model results are in agreement with experimental evidence for nanofiltration membranes and describe the changes of ion retention with pore radius, ion concentrations, pH, and pressure for a binary electrolyte as well as for multicomponent mixtures with cations of different mobility and/or charge. Because protons and hydroxyl ions are taken into account, for the base case markedly different retentions for anions and cations are predicted at pH values below 4 and above 10. A minimum solvent velocity is predicted for a low feed salt concentration of 10–30 mmol/m^3.

NOMENCLATURE

a	pore radius [m]
c_i^{b}	bulk concentration of species i [mol/m^3]
c_i^{e}	concentration of species i in the effluent [mol/m^3]
c_i^{f}	concentration of species i in the feed solution [mol/m^3]
c^{f}	ionic strength [mol/m^3]
c_i^0	concentration of species i at the membrane interface [mol/m^3]
$c_{\mathrm{A}}^{\mathrm{s}}$	concentration of anions at the pore surface [mol/m^3]
$c_{\mathrm{C}}^{\mathrm{s}}$	concentration of cations at the pore surface [mol/m^3]
$c_{\mathrm{H}}^{\mathrm{s}}$	concentration of protons at the pore surface [mol/m^3]
$c_{\mathrm{tot}}^{\mathrm{s}}$	total number of surface sites [mol/m^2]
D_i	Maxwell-Stefan diffusion coefficients at infinite dilution [m^2/s]
F	Faraday constant [C/mol]
K_{A}	anion adsorption equilibrium constant [−]
K_{C}	cation adsorption equilibrium constant [−]
K^+	proton adsorption equilibrium constant [−]
K^-	proton desorption equilibrium constant [−]
K_{w}	water autoprotolysis equilibrium constant [mol^2/m^6]
N_i	molar flux of species i in a fixed coordinate system [mol/(m^2 · s)]
ni	number of ionic species
p	pressure [Pa]
$\mathrm{pH}_{\mathrm{iep}}$	pH at the isoelectric point [−]
R	ideal gas constant [J/(mol · K)]
R_i	retention of species i [−]
r	radial coordinate [m]
T	temperature [K]
v	velocity [m/s]
z	axial coordinate [m]
z_i	charge number of species i [−]
ε_0	dielectric constant of vacuum [C/(V · m)]
ε_{r}	relative dielectric constant [−]
λ	Debye ratio [−]
μ	Newtonian viscosity [Pa · s]
ρ	dimensionless radial coordinate [−]
σ	surface charge [C/m^2]
ϕ	electrostatic potential [V]
ϕ^{s}	electrostatic potential at the pore surface [V]
ψ	dimensionless electrostatic potential [−]
ψ^{b}	dimensionless electrostatic potential in the bulk solution [−]
ψ^{e}	dimensionless electrostatic potential in the effluent [−]
ψ^{s}	dimensionless electrostatic potential at the pore surface [−]
ψ^0	dimensionless electrostatic potential at the membrane interface [−]

REFERENCES

1. Tsuru, T., Urairi, M., Nakao, S.-I., and Kimura, S., *Desalination* **81,** 219 (1991).
2. Jacazio, G., Probstein, R. F., Sonin, A. A., and Yung, D., *J. Phys. Chem.* **26,** 4015 (1972).
3. Basu, S., and Sharma, M. M., *J. Membr. Sci.* **124,** 77 (1997).
4. Sasidhar, V., and Ruckenstein, E., *J. Colloid Interface Sci.* **82,** 439 (1981).
5. Morrison, F. A., Jr., and Osterle, J. F., *J. Chem. Phys.* **43,** 2111 (1965).
6. Gross, R. J., and Osterle, J. F., *J. Chem. Phys.* **49,** 228 (1968).
7. Fair, J. C., and Osterle, J. F., *J. Chem. Phys.* **54,** 3307 (1971).
8. Westermann-Clark, G. B., and Anderson, J. L., *J. Electrochem. Soc.* **130,** 839 (1983).
9. Sonin, A. A., *in* "Charged Gels and Membranes I," p. 255. Reidel, Dordrecht, 1976.
10. Hawkins, Cwirko, E., and Carbonell, R. G., *J. Colloid Interface Sci.* **129,** 513 (1989).
11. Yang, Y., and Pintauro, P. N., *AIChE J.* **46,** 1177 (2000).
12. Deen, W. M., *AIChE J.* **33,** 1409 (1987).
13. Bowen, W. R., and Mukhtar, H., *J. Membr. Sci.* **112,** 263 (1996).
14. Bowen, W. R., Mohammad, A. W., and Hildal, N., *J. Membr. Sci.* **126,** 91 (1997).
15. De Groot, S. R., and Mazur, P., "Non-Equilibrium Thermodynamics," p. 423. Interscience, New York, 1962.
16. Spiegler, K. S., and Kedem, O., *Desalination* **1,** 311–326 (1966).
17. Taylor, R., and Krishna, R., "Multicomponent Mass Transfer," p. 37. Wiley, New York, 1993.
18. Hall, M. S., Starov, V. M., and Lloyd, D. R., *J. Membr. Sci.* **128,** 23 (1997).
19. Hall, M. S., Lloyd, D. R., and Starov, V. M., *J. Membr. Sci.* **128,** 39 (1997).
20. Starov, V. M., Bowen, W. R., and Welfoot, J. S., *J. Colloid Interface Sci.* **240,** 509 (2001).
21. Biesheuvel, P. M., and De Lint, W. B. S., *J. Colloid Interface Sci.* **241,** 422 (2001).
22. Biesheuvel, P. M., *Langmuir* **17,** 3553 (2001).
23. Biesheuvel, P. M., and Lange, F. F., *Langmuir* **17,** 3557 (2001).
24. Ninham, B. W., and Parsegian, V. A., *J. Theor. Biol.* **31,** 405 (1971).
25. Chan, D. Y. C., Perram, J. W., White, L. R., and Healy, T. W., *J. Chem. Soc. Faraday Trans. I* **71,** 1046 (1975).
26. Healy, T. W., Chan, D., and White, L. R., *Pure Appl. Chem.* **52,** 1207 (1980).
27. Healy, T. W., and White, L. R., *J. Colloid Interface Sci.* **9,** 303 (1978).
28. Sasidhar, V., and Ruckenstein, E., *J. Colloid Interface Sci.* **85,** 332 (1982).
29. Takagi, R., and Nakagaki, M., *J. Membr. Sci.* **53,** 19 (1990).
30. He, L. M., Zelazny, L. W., Baligar, V. C., Ritchey, K. D., and Martens, D. C., *Soil Sci. Soc. Am. J.* **61,** 784 (1997).
31. Huang, C. P., and Stumm, W., *J. Colloid Interface Sci.* **43,** 409 (1973).
32. Wesselingh, J. A., Vonk, P., and Kraaijeveld, G., *Chem. Eng. J.* **57,** 75 (1995).
33. Krishna, R., and Wesselingh, J. A., *Chem. Eng. Sci.* **52,** 861 (1997).
34. Bird, R. B., Stewart, W. E., and Lightfoot, E. N., "Transport Phenomena," pp. 149, 196. Wiley, Singapore, 1960.
35. Biesheuvel, P. M., and Verweij, H., *J. Membr. Sci.* **156,** 141 (1999).
36. Biesheuvel, P. M., *J. Colloid Interface Sci.* **238,** 362 (2001).
37. Schaep, J., Vandecasteele, C., Peeters, B., Luyten, J., Dotremont, C., and Roels, D., *J. Membr. Sci.* **163,** 229 (1999).
38. Szaniawska, D., and Spencer, H. G., *Desalination* **101,** 31 (1995).
39. Baticle, P., Kiefer, C., Lakhchaf, N., Larbot, A., Leclerc, O., Persin, M., and Sarrazin, J., *J. Membr. Sci.* **135,** 1 (1997).
40. Yaroshchuk, A. E., Bardot, C., Gaubert, E., Kulov, N. N., and Nechaev, A. N., Modeling of the pressure-driven transport of single and mixed electrolyte solutions across fine-porous inorganic membranes. Criteria for efficient rejection and separation. Presented at ICIM3, Worcester, MA, 1994.
41. Bardot, C., Gaubert, E., and Yaroshchuk, A. E., *J. Membr. Sci.* **103,** 11 (1995).
42. Afonso, M. D., and De Pinho, M. N., *J. Membr. Sci.* **179,** 137 (2000).
43. Zwieniecki, M. A., Melcher, P. J., and Holbrook, N. M., *Science* **291,** 1059 (2001).
44. Grim, E., and Sollner, K., *J. Gen. Physiol.* **40,** 887 (1957).
45. Kobatake, Y., and Fujita, H., *Kolloid Z.* **196,** 58 (1963).
46. Atkins, P. W., "Physical Chemistry," 4th ed., p. 171. Oxford Univ. Press, Oxford, 1990.
47. Cussler, E. L., "Diffusion. Mass Transfer in Fluid Systems," p. 147. Cambridge Univ. Press, Cambridge, 1984.